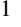


Pure Gravitational Wave Estimation of Hubble’s Constant using Neutron Star - Black Hole Mergers

Leo W.H. Fung,¹  Tom Broadhurst,^{2,3,4} George F. Smoot^{1,3,5,6,7}

¹ Department of Physics and Jockey Club Institute for Advanced Study, Hong Kong University of Science and Technology, Hong Kong

² University of the Basque Country UPV/EHU, Department of Theoretical Physics, Bilbao, E-48080, Spain

³ DIPC, Basque Country UPV/EHU, San Sebastian, E-48080, Spain

⁴ Ikerbasque, Basque Foundation for Science, Bilbao, E-48011, Spain

⁵ Energetic Cosmos Laboratory, Nazarbayev University, Nursultan, Kazakhstan

⁶ APC; AstroParticule et Cosmologie, Université de Paris, Paris Centre for Cosmological Physics, CNRS/IN2P3

CEA/Irfu, 10, rue Alice Domon et Leonie Duquet, 75205 Paris CEDEX 13, France Emeritus

⁷ Physics Department & LBNL, University of California at Berkeley CA 94720 Emeritus

Accepted XXX. Received YYY; in original form ZZZ

ABSTRACT

Here we show how H_0 can be derived purely from the gravitational waves (GW) of neutron star-black hole (NSBH) mergers. This new method provides an estimate of H_0 spanning the redshift range, $z < 0.25$ with current GW sensitivity and without the need for any afterglow detection. We utilise the inherently tight neutron star mass function together with the NSBH waveform amplitude and frequency to estimate distance and redshift respectively, thereby obtaining H_0 statistically. Our first estimate is $H_0 = 86^{+55}_{-46}$ km s^{−1} Mpc^{−1} for the secure NSBH events GW190426 and GW200115. We forecast that soon, with 10 more such NSBH events we can reach competitive precision of $\delta H_0/H_0 \lesssim 20\%$.

Key words: Cosmological parameters – Gravitational waves – Methods: observational – distance scale

1 INTRODUCTION

Knowledge of the expansion rate of the universe is essential for deriving the physical characteristics of extragalactic objects, including sizes and masses of galaxies and clusters and the age and luminosity of their stellar contents. Increasingly precise standard candles and rulers have revealed the Hubble expansion has actually accelerated over the past few Gyrs, indicating a constant energy density with negative pressure governs the expansion rate today. As H_0 measurements have improved in precision, consistent claims that smaller values of H_0 have been inferred from distant cosmological measurements compared with local estimates of H_0 from the stellar calibrated standard candles (Scolnic et al. 2018; Riess et al. 2021; Verde et al. 2019; Knox & Millea 2020). A careful recalibration of local cepheids is now claimed to slightly relieve this H_0 tension when supernovae are classified according to metallicity, or from recalibration of evolved stars at the tip of red giant branch (Freedman et al. 2019; Freedman et al. 2020) (and see Freedman (2021) for a review).

Alternatively, theoretical proposals to explain the Hubble Tension include a re-interpretation of the cosmic microwave background (CMB) data, invoking the modifications of recombination physics (for a review Valentino et al. (2021)), may allow the ‘standard’ sound horizon scale length to be slightly smaller, by shifting the surface of last scattering to a little earlier in time, corresponding to a higher redshift allowing agreement with the local H_0 estimates. It has been shown this may be achieved by modifying recombination physics (Fung et al. 2021, 2023; Luu 2021; Jedamzik et al. 2021; Ivanov

et al. 2020) that shifts the calibration, allowing room for reinterpreting the data with a somewhat higher H_0 .

The seemingly irreconcilable differences among H_0 measurements obtained from different ‘standardizable’ calibration (candles and rulers) strengthen the need for measuring H_0 with independent methods with calibrations driven by unrelated physical mechanisms. Gravitational wave (GW) observations provide exciting new opportunities for constraining such cosmological expansion. Compared to conventional electromagnetic (EM) observations where flux falls as the square of the luminosity distance, the GW signal strength scales only linearly inverse with luminosity distance – as the detected strain amplitude depends on the square root of energy density per unit time. As a result, the scaling of GW signal strength can be used to distinguishing models that involve modification of photon trajectories (consequently modifying the cosmic distance duality relation (Etherington 1933; Bassett & Kunz 2004)), or other proposals that introduce strongly redshift dependent physics (for example Camarena & Marra (2021)).

Aside from the unique scaling of signal strength, there are also some applications of GW that depend on physical assumptions lying outside gravitational wave data and consequently, such methods do not fully benefit from the new GW-based window. It has been proposed that spatial cross correlations between GW sources and galaxy surveys can provide a ‘siren’ based angular scale that does not rely on individual (unknown) GW host galaxy identification. By using galaxy redshift surveys of suitable depth (Mukherjee et al. 2021; Cigarrán Díaz & Mukherjee 2022; Oguri 2016) and all BBH events to date a value of $H_0 = 68^{+8}_{-6}$ kms^{−1} Mpc^{−1} has been estimated. This rests on a statistical comparison of the ensemble of BBH sky location

* leowhfung@gmail.com

areas with the Dark Energy Survey (DES) optical galaxy survey as no unique host galaxy identification (LVK, 2021a) is yet possible. Hence, this type of method that relying on the establishment of a standard ruler in general shares almost the same set of systematic problems as traditional standard ruler approaches, in particular the baryonic acoustic oscillations and as a result, the GW data does not represent a truly independent means for constraining H_0 . For the consideration of Hubble tension, this would be unable to offer an independent check of the systematics. To overcome this limitation, we propose to rely on pure GW emission, as described below.

The long anticipated GW-based method to constrain H_0 using binary neutron stars, pioneered by (Schutz 1986), falls in the ‘standard candle’ class and requires a prompt detection of nova emission generated during the merger, to define the redshift. This method has finally been realised with the first GW detection of a BNS event GW170817, for which there is an optical redshift (LIGO-Virgo; LIGO-Virgo, 2017a; 2017b). Fortunate Fermi satellite detection of prompt gamma-ray emission from associated kilonova emission has localised the host galaxy, providing an optical spectroscopic redshift for the host. The recession velocity of the host galaxy is only 3000 km s^{-1} requiring a sizeable peculiar motion correction, at an estimated level of $\approx 800 \text{ km s}^{-1}$, resulting in $H_0 = 70^{+12}_{-8.0} \text{ km s}^{-1} \text{ Mpc}^{-1}$. The uncertainty on this estimate brackets the disputed range of H_0 , and implies approximately 10 more such BNS events are required to address independently the current H_0 tension between SN-Ia and the CMB/Large Scale Structure (LSS) based estimates (Nissanke et al. 2013). However, such coincident, multi-messenger observations are not anticipated to be available frequently, unless the angular resolution of GW observatories can be drastically improved (by ~ 3 orders of magnitude) to localized the position of the event, and indeed subsequent events classified as BNS were not detected at other wavelengths in prompt follow-up searches.

These GW based methods for H_0 rely on an independent EM based redshift estimation, either individually in the case of BNS mergers or statistically with redshift surveys described above.

A pure GW based method for estimating H_0 has been proposed for the future, requiring much improved sensitivity, when the tidal deformation of the NS by the BH during a NSBH merger is detectable. This can provide in principle a GW based estimate of H_0 from the additional distance dependence on this physical deformation (Chatterjee et al. 2021). Here we propose another more practical ‘standard’ strain pure GW method, that has apparently been overlooked, provided by the inherently narrow NS mass function established by radio, X-ray and optical observations in the Milky Way and local group, including binary neutron star pulsars.

We will show below that the GW radiation from neutron star-black hole (NSBH) binaries, rather than BNS events, is more suitable for the purpose of derive a reliable estimate of H_0 , free from local peculiar motions that introduce model dependence for BNS estimates. We apply this method to the currently secure NSBH event GW200115 and other possible and proposed candidate NSBH events variously reported. We demonstrate that the existing instruments (LIGO collaboration 2020) already suffice for constraining H_0 within $\delta H_0/H_0 \lesssim 20\%$ simply by gathering 10 years of measurements, even in the absence of significant sensitivity upgrades that may be anticipated. We will emphasize throughout that NSBH events and to a lesser extent BNS events, can in combination provide competitive precision on H_0 that is purely derived from the GW radiation alone, without the need for a spectroscopic redshift. Such additional independent information would of course provide further improvement, so that this combined general NS based estimate of H_0 we can anticipate will prove useful in practice.

Our paper is organized as follows: in Section 2, we sketch out the basis of the method, and then we describe our choice of datasets for GW events and local X-ray binaries in Section 3. We present a rigorous Bayesian hierarchical analysis applied to the data in Section 4 and preset our analysis of the first reported GW events compatible with being NSBH binaries, focusing in particular on the secure NSBH detection claimed to date, GW200115 (LVK, 2021) for a first estimate of H_0 . We then make a forecast for the precision attainable for H_0 , and the evaluation of associated systematics in Section 5. We finally conclude in Section 6.

2 INTUITIVE OVERVIEW OF THE METHOD

The widely applied standard candle measurement of H_0 compares independently determined luminosity distances, d_L , with spectroscopic redshifts, z , for type-Ia supernovae where luminosity is calibrated with local Cepheids. Here we emphasises that a pure GW based measure of H_0 is now feasible without the need for a follow-up spectroscopic redshift. Owing to stellar stability constraints, the mass range of neutron stars is fairly tight about the Chandrasekhar mass. Hence the lower mass binary member (neutron star) modulation of the NSBH waveform is predictable, so the degeneracy between luminosity distance and redshift of NSBH is relatively small. Consequently GW detections alone provide useful measurements of both d_L and z and hence a statistical measure of H_0 , as we outline below. This method we apply to GW waveforms identified as NSBH binaries, where the mass ratio can be defined from the waveform modulation and the presence of the relatively massive BH extends the detection horizon to $z \lesssim 0.25$, large enough for statistical measure of H_0 .

2.1 Observables

For our purposes we require only the time varying GW strain amplitude and phase registered by the laser interferometers, rather than relying on the template fitted waveform derived parameters reported for the GW detections. We emphasize here non-parametric (independent of source model) summary statistics that can be used to approximately describe the waveform below with post-Newtonian (PN) calculations that allow us to describe the physical quantities of the GW source with the summary statistics. Below, we will use the subscript $_{\text{obs}}$ to denote these non-parametric statistics.

The amplitude of the strain h_{obs} according to the post-Newtonian (PN) calculations (Poisson & Will 1995; Ajith et al. 2008) for compact binary sources is given by the following combination of physical parameters:

$$h_{\text{obs}} \propto \frac{((1+z)\mathcal{M}_c)^{5/6}}{d_L} \quad (1)$$

The $(1+z)$ factor can be understood as follows: as h_{obs} scales with $\sqrt{\text{Energy}}$, the rate of radiation energy received by the observer is time dilated by the cosmological redshift. Also, the inverse square law $1/d_L^2$ diffusion of energy (flux) implies an inverse dependence of h_{obs} on luminosity distance d_L . Hence, to determine d_L , we therefore need another observable, ideally independent to h_{obs} , to pin down $(1+z)\mathcal{M}_c$. If we take the fourier transform of the time series of strain over different time windows (for example, Q-transform), the time evolution of the corresponding frequency spectrum can also be determined.¹ The first quantity is the redshifted chirp mass

¹ The situation is more complicated when the signal is contaminated by

$(1+z)\mathcal{M}_c$. The chirp mass is defined as:

$$\mathcal{M}_c \equiv \frac{(m_1 m_2)^{3/5}}{(m_1 + m_2)^{1/5}} = \frac{1/q^{3/5}}{(1+1/q)^{1/5}} m_2, \quad (2)$$

where we have defined the mass ratio $q = m_2/m_1$, and implicitly by definition $m_2 < m_1$ for sorting the masses in the binary system. This quantity, upon redshifted, is indeed imprinted on the spectral moment of the 0.5PN chirping spectrum $f_{\text{obs}}(t)$: (note however, that solving the spectral evolution must be done by solving the full differential equation, and the order-by-order approach as outlined below only make sense under some strict conditions.²)

$$f_{\text{obs}}^{-11/5} \left(\frac{df_{\text{obs}}}{dt} \right)^{3/5} \sim (1+z)\mathcal{M}_c. \quad (3)$$

The redshift effect is easy to understand: the frequency of GW in the source frame is redshifted to $(1+z)^{-1}f_{\text{obs}}$ and thus the time derivative $(1+z)^{-1}df_{\text{obs}}/dt$. If we can pin down m_2 and q , it would then be possible to estimate z . Indeed, considering NSBH system, the neutron star mass m_2 can be pinned down by Milky Way observations as $m_2 = 1.4 \pm 0.1 M_\odot$ (see Section 3 for the evidence of this number).

On an order-by-order basis, it is also possible to determine the mass ratio q by another combination of spectral evolution:

$$f_{\text{obs}}^{-13/3} \frac{df_{\text{obs}}}{dt} \sim \frac{1/q}{(1+1/q)^2}, \quad (4)$$

where all the redshift dependencies are cancelled by the multiplicative scaling term that we have neglected here. (Poisson & Will 1995)

³ Therefore, this observable provides a measurement on q .

We summarize the relations between the observables and physical source quantities in Fig. 1. Clearly, the observed quantities provide largely independent measurements of z and d_L respectively. The $(z_i, d_{L,i})$ pairs from each observed NSBH event i can therefore be used to determine the Hubble constant H_0 . In the big bang cosmology, we have:

$$\frac{d_L}{(1+z)} = \frac{c}{H_0} \int_0^z \frac{dz'}{E(z')}. \quad (5)$$

In the subsequent numerical analysis, we will assume $\Omega_m = 0.3$, so that $E(z) = \sqrt{0.3(1+z)^3 + 0.7}$, as the current data quality does not allow strong constrain on Ω_m together with H_0 .

2.2 Comparison with Binary Neutron Star events

Here we compare and contrast the ability of BNS and NSBH events for estimating H_0 by the method proposed here, including BNS events that do not have an independent spectroscopic redshift estimate because no host galaxy nor EM emission is identified. The absence of observed EM counterparts likely comprises the majority of such

noise, where parametric models of the GW waveform are used as matched filters for deriving the waveform evolution. We will ignore this point in this section for illustration.

² Strictly speaking, the spectral moments cannot be separated in this way. However, by using multi-scale perturbation methods (for example, Poincaré-Lindstedt), the order-by-order separation can be a good approximation in a narrow time window, where the window time scale is defined by the leading coefficients of each spectral moment.

³ Precisely, the spectral evolution df_{obs}/dt couples with the polynomial in f_{obs} . As a result, the combination of moments of the spectrum are not orthogonal to each other. The full PN calculation for relating the observables to the chirp spectrum can be found in the pioneering work (Poisson & Will 1995) (in particular Eq.1.3 therein) and for accurate estimation the spectrum must be predicted numerically using ODE solvers.

NS related GW events given the follow-up success to date, with EM emission found for just one very local BNS event, at only 40 Mpc and the absence of EM detections for the other BNS and NSBH candidates.

One may argue BNS systems are more suitable for the purpose of establishing an independent estimate on z and thus H_0 . This is seemingly evident from Eq.2: if both $m_{s,1}$ and $m_{s,2}$ are pinned down, \mathcal{M}_c are known a priori. There are though two advantages for NSBH events compared to BNS in terms of realising our H_0 method. Firstly, the detection horizon for NSBH observations is much larger than is BNS observations. As shown in (Ajith et al. 2008), the signal-to-noise ratio (SNR) of GW events scale as $\rho(m_{s,1}, m_{s,2}, z) \sim \frac{((1+z)\mathcal{M}_c)^{5/6}}{d_L(z)}$. For BNS with mass ratio $q \approx 1$, $\mathcal{M}_c \approx 0.87m_2$; whereas the BH component serves as an efficient amplifier, boosting the detectable SNR of the companion NS: on average, the BH mass can be as high as $m_{s,1} \approx 20M_\odot$, corresponding to an amplification factor of $1/q \approx 13$. Thus $\mathcal{M}_c \approx 2.75m_2$, thereby extending the detection horizon for NSBH events to $d_L^{(\text{NSBH})}/d_L^{(\text{BNS})} \approx 4$, four times times larger than BNS events.

The larger horizon depth for NSBH event detection relative to BNS events can be translated into an improvement in H_0 via a simple Fisher information argument. Roughly the likelihood for H_0 follows a Gaussian $\mathcal{G}(d_L; \hat{d}_L(z; H_0), \sigma_d)$, where the expected luminosity distance \hat{d}_L at redshift z is parameterized by H_0 , subjected to distance measurement uncertainty σ_d . The Cramor-Rao bound states the propagation of uncertainty to H_0 is roughly (with the angled bracket denotes ‘taking expectation’ from the distribution):

$$\delta H_0 \geq \left\langle \frac{\partial \log \mathcal{G}^2}{\partial H_0} \right\rangle_{\sim d_L}^{-1/2} = \left\langle \left(\frac{\partial \log \mathcal{G}}{\partial \hat{d}_L} \frac{\partial \hat{d}_L}{\partial H_0} \right)^2 \right\rangle_{\sim d_L}^{-1/2} \sim \sigma_d H_0 \frac{1}{\hat{d}_L}, \quad (6)$$

where δH_0 denotes the standard deviation of the H_0 posterior. Therefore, δH_0 scales (at leading order) as $1/\hat{d}_L$: the enlarged horizon allows more amplification of the difference between a static universe and an expanding universe, hence helping to shrink the uncertainty in H_0 , provided that the distance measurement uncertainty σ_d scales slower than \hat{d}_L .

The enlarged detection horizon is also beneficial in terms of the precision in pinning down the cosmological redshift. In practice, the measured redshift is contributed by both the cosmological expansion and the local peculiar motion. When the fractional redshift error is assessed, a low detection horizon would be translated to a larger fractional redshift uncertainty. This effect can be mitigated by making the peculiar motion-induced redshift contributes only a tiny portion of the total redshift, effectively by using the GW emission at farther distance.

The second advantage for NSBH over BNS events comes from the absolute uncertainty in determining the mass ratio $q \equiv m_{s,2}/m_{s,1}$, which is smaller with $1/q \gg 1$ for NSBH events where the waveform is typically extended in time providing an accurate orbital definition. Consequently, this enables more accurate measurements of the 0.5PN signal on q via monitoring the time evolution of the frequency spectrum (i.e.: chirping). As the uncertainty in $m_{s,2}$ is rather fixed by the intrinsic scatter of the NS mass function, the significant reduction in δq implies a tighter constraint in the redshifted-chirp mass $(1+z)\mathcal{M}_c$, and consequently in d_L . For BNS systems $q \approx 1$ and thus the mass ratio is relatively less well constrained by the data, leading to significant H_0 uncertainty, whereas the tight prior restriction from

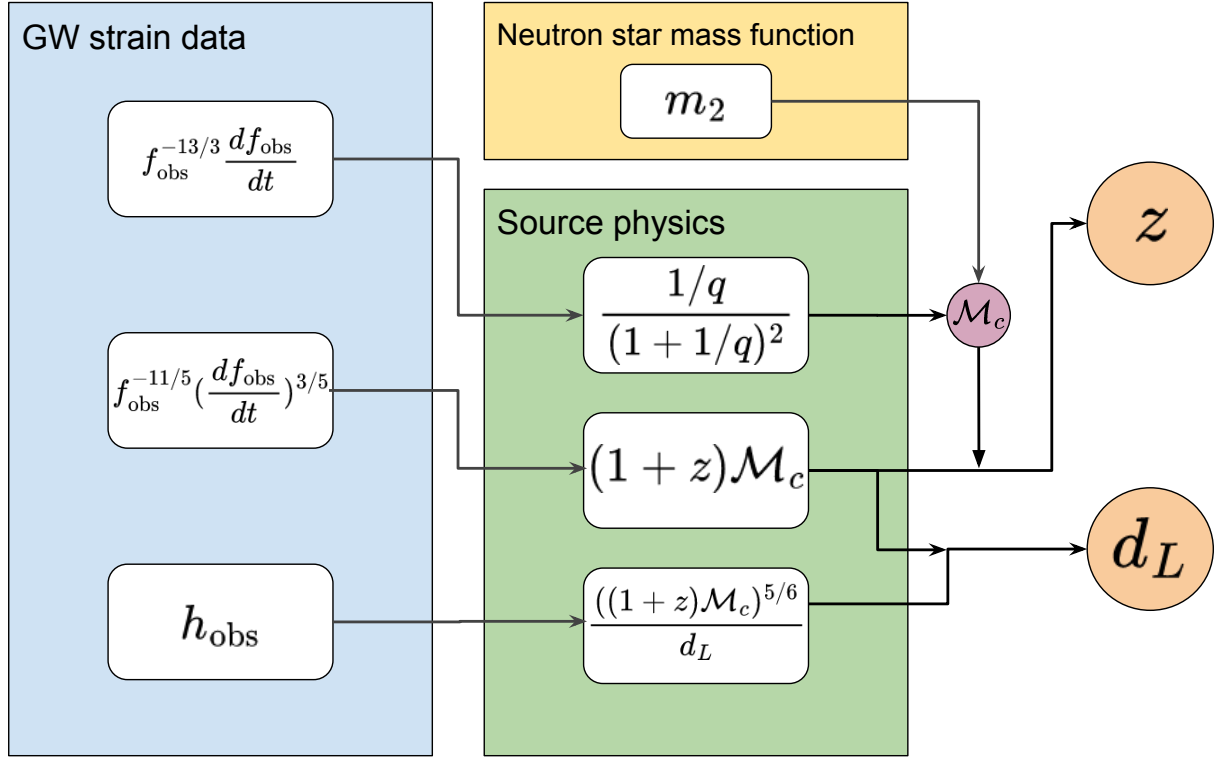


Figure 1. Summary of the relations between observables and the physical quantities of the GW source, and the associated relation to quantities of cosmological interest.

the NS mass function instead provides a desirable tight prior on the source frame chirp mass \mathcal{M}_c for BNS events.

We will examine the difference between NSBH and BNS events in detail using simulation in Section 5.1.

3 DATA

3.1 NSBH Mass function in the Milky Way

The initial birth masses of neutron stars are predicted to lie in the range, $M_{\text{birth}} \sim 1.08 - 1.57 M_{\odot}$, depending on the modeling of the underlying hydrodynamical processes and thermodynamics with subsequent evolution. In the case of close binaries, as neutron stars accrete material from companions, leading to a dependence of the NS mass on the physical properties of the secondary, companion star. The upper limiting mass of a NS star is also understood to sensitively depend on uncertain nuclear reactions and also rotation rate affecting the equation of state (Kiziltan et al. 2010), under physically extreme nuclear conditions, allowing unique tests of the standard model in conditions as yet unrealized in the laboratory.

Fortunately for our purposes the empirically determined NS mass function is well defined, with an inherently narrow spread of masses. Decades of observations have established that the majority

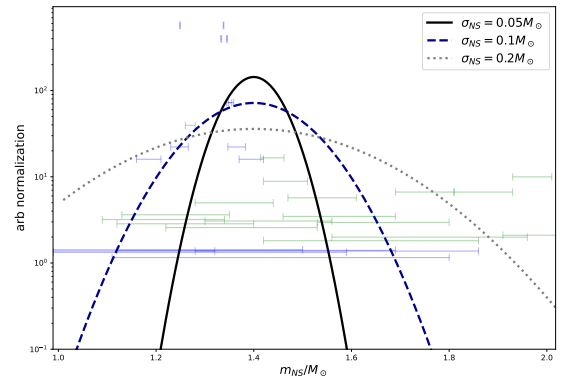


Figure 2. The EM-observed masses of neutron stars in a double neutron star system (in blue) and neutron star-white dwarf systems (in green), compiled in (Kiziltan et al. 2010). We also plot the 3 fiducial model of the underlying neutron star mass function - as a Gaussian with a peak at $\langle m_{\text{NS}} \rangle = 1.4 M_{\odot}$ and with various variance as shown in the legend.

of neutron stars have masses consistent with a single mass scale of $\langle M_{\text{NS}} \rangle = 1.4M_{\odot}$, coinciding with the classically predicted for a universal iron core (Lattimer 2012), including over ~ 50 radio pulsars (Thorsett & Chakrabarty 1999). Hence, we first adopt this empirically well defined prior mass function, approximately described simply by a Gaussian centered at $\langle M_{\text{NS}} \rangle = 1.4M_{\odot}$, and consider an intrinsic spread of NS mass ranging over $\sigma_{\text{NS}} \in [0.05, 0.2]M_{\odot}$ in our subsequent analysis below. A possible bimodal mass distribution for Galactic neutron stars has been claimed in recent analyses for a classification by the type of binary companion, (Kiziltan et al. 2010) and fitted to two Gaussians with of differing mean mass and variance. For binary NS systems, a mean NS mass of $\langle M_{\text{NS}} \rangle = 1.35M_{\odot}$ is claimed to be significantly smaller the mean NS mass of NS-white dwarf binaries, estimated to be $\langle M_{\text{NS}} \rangle = 1.5M_{\odot}$ and with a smaller spread in mass. Other classifications are also proposed (Kiziltan et al. 2013) that do not separate companion types (Valentim et al. 2011) (see (Horvath & Valentim 2017) for a review of recent progress of constraining NS mass function), may also suggest two separated mass peaks with masses similar to (Kiziltan et al. 2010; Zhang et al. 2011). We replot the EM-observed NS mass data from (Kiziltan et al. 2010) in Figure 2, along with the 3 fiducial models of the NS mass function that we would use throughout this analysis. We emphasize that our framework of analysis can be easily adopted to any NS mass function and in considering a binary mass distribution. We find that the H_0 posterior inferred from such a simple Gaussian model does not significantly differ from adopting a more complicated NS mass function, so that our H_0 forecast is insensitive to the details of the NS mass function given the GW data quality anticipated. This argument would be verified in Section 5.

Lastly, there is also evidence from the gamma-ray that there can be some NS-like compact objects with relatively high masses (Romani et al. 2012), with an upper extreme of $M_{\text{NS}} \lesssim 2.3M_{\odot}$ established empirically recently for the well studied ‘black widow’ pulsar PSR B1957+20 (Fruchter et al. 1988) (and a more recent analysis (Kandel & Romani 2022)). The abundance of these relatively massive MS pulsars are much lower than the ‘classical’ population at $\langle M_{\text{NS}} \rangle \pm \sigma_{\text{NS}}$ and these massive examples appear separated from the ‘classical’ population tightly clustered around $1.4M_{\odot}$, allowing the possibility of excluding this uncertain, massive population from our analysis, so we may restrict ourselves to the predominant NS population both in calibrating the NS mass distribution and in comparison to the NSBH events observed from the GW channel. We anticipate that as long as we consistently exclude conspicuously massive NS related events that this prior selection will not induce a significant bias in our subsequent analysis.

3.2 Gravitational Waves from NSBH events.

The LIGO-Virgo-Kagra collaboration (LVK) completed a third observational run in March 2020 and released the GWTC-3 catalog (LVK, 2021b), containing 90 observed binary coalescence events. The majority are classified as binary black holes mergers (BBH), with initially two events classified as neutron star-black hole mergers (NSBH) (LVK, 2021). Subsequently only one of these events GW200115 has survived scrutiny and now reported in the combined final catalogue (LVK, 2021b). An earlier event initially classed as BBH may now conform better to the NSBH definition, as we tentatively argue below, namely GW190426.

The identification of NSBH events is predominantly based on the observed secondary mass $m_{o,2} = (1+z)m_{s,2}$, unlike BNS events. In principle, NSBH can produce a more complicated waveform than is BBH due to the tidal deformation of the NS, however the current data

quality does not yet able to constrain such higher order tidal effects (Chatterjee et al. 2021). Therefore the claimed NSBH event(s) mostly rest on a low secondary mass estimated to lie below a maximum of $m_{o,2} \lesssim 2.5M_{\odot}$. In Table 1, we list all the reported candidate events, including their posterior mean primary masses $m_{o,1} > 5M_{\odot}$ and secondary masses $m_{o,2} < 2.5M_{\odot}$, comprising a total of 5 events satisfying this criterion. These events are in general of relatively low SNR (as the SNR scales almost linearly with chirp mass), but is compensated to some extent by the better instrumental sensitivity at higher frequencies. GW events with $m_{s,2} = 2.6M_{\odot}$ (GW190814) and $m_{s,2} = 2.8M_{\odot}$ (GW200210) have been reported in GWTC-3. Some of us have discussed these separately in the context of possible lensing of NSBH events that allows detection at higher redshift where the chirp mass is enhanced significantly by $(1+z)$ (Broadhurst et al. 2020). Furthermore, as will be shown in Section 5, the robustness of our method is not strongly influenced by the inclusion or the exclusion of such high mass events.

In Table 1 we indicate the status of the 5 possible NSBH candidate events reported to date. (We would only quote the GW in the table by the first half name of the event, ignoring the ID behind the underscore.) Three of these are reported as marginal, including GW190426 with a high false alarm rate 32 yr^{-1} in the MBTA pipeline, first reported in the GWTC-2.1-marginal catalog. (Aubin et al. (2021), LIGO-Virgo (2021)) As commented by LVK (LIGO-Virgo, 2021), such a high false alarm rate is mainly attributed to the initially low NSBH event rate adopted by prior expectations based on the absence of NSBH events, that may be regarded as a somewhat circular argument resulting in the probability of an astrophysical origin assigned to this event of $p_{\text{astro}} \leq 0.12$ across all the analysis pipelines. Hence, this ‘prior’ may now be revised upward in retrospect with the subsequent confident identification of GW200115 as an NSBH event. The event GW191219 is also a marginal detection with a high false alarm rate of 4.0 yr^{-1} , and the secondary mass in the source frame is relatively low mass $m_{s,2} < 1.2M_{\odot}$ at 68% credibility. This marginal event is also with by far the most extreme mass ratio $q = 0.04^{+0.005}_{-0.007}$ among the observed events, raising further doubt about its viability as real astronomical event and this is why it flagged as by the LVK as marginal ((LVK, 2021b) Table II).

A third marginal NSBH candidate event is GW200105 of low SNR, partially due to LIGO Hanford was offline at the time of detection. The only detector that reached the desired SNR is the LIGO Livingston (LVK, 2021), where a chirping signal are clearly observed when the data stream are plotted on a Q-transform spectrogram. (LVK, 2021). Despite the relatively strong SNR= 13.9 reported in (LVK, 2021b), the event has a $p_{\text{astro}} = 0.36$. For this reason, this event is classified as marginal by the LVK in (LVK, 2021b).

This leaves two NSBH candidates, including GW200115, which has been consistently classed by the LVK as a secure NSBH event (LVK, 2021), whereas the earlier revised detection GW190426 which although not classed as NSBH or claimed as such does seem to satisfy the NSBH requirement in terms of the security of its detection and the reported component masses. So we focus on these two events here and in particular, GW200115 given the secure status of this NSBH event as claimed by the LVT (LVK, 2021).

4 STATISTICAL FRAMEWORK

Throughout the paper we use the notation $\pi(\cdot)$ to denote the prior distribution, in contrast to the probability distribution $p(\cdot)$ to describe relations among the model parameters and the data.

Event ID	$m_1(1+z)/M_\odot$	$m_2(1+z)/M_\odot$	$M(1+z)/M_\odot$	q	d_L/Mpc	Ref.
GW190426_152155	$6.45^{+1.07}_{-1.78}$	$1.61^{+0.24}_{-0.34}$	$2.60^{+0.007}_{-0.006}$	$0.28^{+0.05}_{-0.15}$	394^{+105}_{-109}	LIGO-Virgo (2021) Aubin et al. (2021); Li et al. (2020)
GW190917_114630	$11.2^{+2.08}_{-2.46}$	$2.45^{+0.24}_{-0.50}$	$4.21^{+0.014}_{-0.018}$	$0.24^{+0.03}_{-0.12}$	740^{+173}_{-195}	LIGO-Virgo (2021)
GW191219_163120	$33.2^{+2.44}_{-3.61}$	$1.35^{+0.07}_{-0.08}$	$4.81^{+0.021}_{-0.045}$	$0.04^{+0.005}_{-0.007}$	682^{+187}_{-168}	LVK (2021b)
GW200105_162426	$9.26^{+1.07}_{-1.64}$	$2.11^{+0.19}_{-0.28}$	$3.62^{+0.005}_{-0.007}$	$0.24^{+0.04}_{-0.08}$	$283^{+79.6}_{-76.7}$	LVK; LVK (2021b; 2021) ⁴
GW200115_042309	$6.82^{+1.13}_{-1.26}$	$1.48^{+0.13}_{-0.25}$	$2.58^{+0.004}_{-0.004}$	$0.23^{+0.04}_{-0.09}$	$283^{+62.1}_{-82.7}$	LVK; LVK (2021b; 2021)

Table 1. List of candidate NSBH events. We list the reported observed frame quantities here, rather than the more model dependent source frame quantities as shown in the table compiled by LVK (LVK, 2021b). The uncertainty ranges are the 68% highest posterior density intervals. Remarkably, the uncertainty are correlated and clearly visible in terms of $q \equiv m_2/m_1$: where the error bar on this mass ratio is much smaller than $m_1(1+z)$ and $m_2(1+z)$. Values shown are only for quick reference; we use the full posterior samples in deriving these summaries, and similarly in all the subsequent analysis and only the events in **bold font** are regarded as reliable for the the analysis in this paper, in reference to the reported reliability of the classification of these events, as described in Section 3

4.1 H_0 posterior

We aim here to find the posterior for H_0 given the event waveforms, $\{D_i\} \equiv \bigcup_i D_i$, namely $p(H_0|\{D_i\})$. For each event with observed waveform D_i , the LVK collaboration has fitted a cosmology-free event-level posterior $p_i(d_L, z, \theta|D_i)$, with θ are the remaining event level parameters (excluding d_L and z). We wish to ‘sum’ all the events properly to infer the (population-level) value of H_0 .

To avoid *ab initio* fitting, we use the following reweighing scheme as proposed originally for galaxy morphology dataset in (Hogg et al. 2010), and employed subsequently in GW analyses (Mandel et al. 2019b). The posterior can be rewritten using Bayes theorem to flip H_0 as the condition, and expand the marginalized event level parameters as:

$$\begin{aligned}
 p(H_0|\{D_i\}) &\propto \pi(H_0) \int p(\{D_i\}|d_L, z, \theta) p(d_L, z, \theta|H_0) dd_L dz d\theta \\
 &= \pi(H_0) \prod_i^{N_{\text{obs}}} \int p(D_i|d_L, z, \theta) p(d_L, z, \theta|H_0) dd_L dz d\theta.
 \end{aligned} \tag{7}$$

The next step is to invoke the Bayes theorem to rewrite $p(D_i|d_L, z, \theta)$:

$$p(D_i|d_L, z, \theta) = \frac{p(d_L, z, \theta|D_i, \text{LVK})p(D_i|\text{LVK})}{p(d_L, z, \theta|\pi_{\text{LVK}})}, \tag{9}$$

with $p(d_L, z, \theta|\pi_{\text{LVK}})$ being an uninformative parameter prior adopted by LVK. Following a similar notation, the term $p(d_L, z, \theta|D_i, \text{LVK})$ represent the parameter fitting results when the LVK uninformative prior is used to fit the data. For a similar reason, the term $p(D_i|\text{LVK})$ is an uninformative data prior, which is mathematically equal to a constant, and could be absorbed as an overall normalization constant. In general, these terms can have non-trivial form to account for the selection bias as well, and we will elaborate this in Section 4.3.

Note the K_i sample points of the posterior $p(d_L, z, \theta|D_i, \text{LVK})$ are available in the LVK data releases. Using these samples, one can rewrite Eq. 7 as:

$$p(H_0|\{D_i\}) \propto \pi(H_0) \prod_i^{N_{\text{obs}}} \frac{1}{K_i} \left[\sum_{\sim \theta, d_L, z}^{K_i} \frac{p(d_L, z, \theta|H_0)}{p(d_L, z, \theta|\pi_{\text{LVK}})} p(D_i|\text{LVK}) \right], \tag{10}$$

where the integration $\int dd_L dz$ is replaced by the Monte-Carlo sum $\frac{1}{K_i} \sum^{K_i}$. As argued above, every term except $p(d_L, z, \theta|H_0)$ in the square bracket can be modelled as an overall multiplicative constant. The data fitting results come into the above likelihood function via

the Monte Carlo summation \sum , while the goodness of fit to the model is assessed in the term inside the Monte Carlo sum. In the subsequent subsection, we would explain how the goodness of fit term can be formulated.

4.2 Redshift-distance Likelihood

There is a non-trivial point about the MCMC samples released by LVK. Despite values of redshift z are reported in the MCMC chain, those reported value of z should be interpreted with extra care - indeed, their face values are not applicable to our application at all.

The LVK fitting pipeline does not fit for the $(1+z)$ factor directly as it is completely degenerate with the restframe chirp mass Eq. 3 in terms of the frequency response behaviour. Instead, the LVK pipeline utilized the Planck cosmology (Planck Collaboration et al. 2020) with $H_0 = 67.9 \text{ km s}^{-1} \text{ Mpc}^{-1}$, so that the luminosity distance d_L that parametrized the GW waveform is directly converted to the redshift, and these directly converted values of z are reported in the MCMC chain. Therefore, the MCMC samples from LVK collaboration are samples of $\{d_L, m_{o,2}, \theta\}$ instead of directly containing z ⁵

For this reason, all the probabilities containing z in Eq. 10 must be replaced by $m_{s,2}$, which indirectly constrain z with the use of the Milky Way NS mass function.

Our prior here is the independent knowledge of the distribution of $m_{s,2}$ from the long standing Milky Way NS mass distribution, which we can factorize and write H_0 likelihood (the term inside the bracket in Eq. 10) as:

$$\begin{aligned}
 p(m_{o,2}, d_L, \theta|H_0) &= \int dz dm_{s,2} d\beta p(m_{o,2}|z, m_{s,2}) p(d_L|z, H_0) \\
 &\quad \times p(z|\beta) \pi(m_{s,2}) \pi(\theta) \pi(\beta)
 \end{aligned} \tag{11}$$

It is clear how the information regarding z indirectly comes into the expression: if $m_{s,2}$ are known precisely, $z = m_{o,2}/m_{s,2} - 1$ would inherit the data uncertainty in $m_{o,2}$. The above equation simply takes the intrinsic scatter of $m_{s,2}$ into account, promoting $m_{s,2}$ to a probability $\pi(m_{s,2})$.

Note the conditionals $p(m_{o,2}|z, m_{s,2})$ and $p(d_L|z, H_0)$ (i.e.: the

⁵ There is a ‘no-cosmology’ MCMC sample chain available in the LVK data release. However, the interpretation of ‘no-cosmology’ is also different from what we are doing in this paper. In fact, their ‘no-cosmology’ chain only means excluding a volumetric prior for event rate. The convention of assuming $h = 0.679$ to convert d_L to z directly is still held in this ‘no-cosmology’ chain. Therefore this chain cannot be used directly without using the likelihood marginalization method we presented in this paper. See Appendix A for more detailed description for reproducing the results we shown here.

first two terms before the multiplication symbol) are deterministic, and are thus possible to be expressed in terms of Dirac delta. This simplifies the expression to:

$$p(m_{o,2}, d_L, \theta | H_0) = \int d\beta p(z = z(d_L; H_0) | \beta) \times \pi(m_{s,2} = m_{o,2} / (1 + z(d_L; H_0))) \pi(\theta) \pi(\beta) \quad (12)$$

While the inverse function $z(d_L; H_0)$ does not admit an analytical form, a computationally inexpensive numerical solution can be easily obtained because $d_L(z; H_0)$ is a monotonic function of z . When d_L is known and a fixed value of H_0 is chosen in a MCMC sampling step, the corresponding value of $z(d_L, H_0)$ is uniquely determined. And the likelihood of generating this specific $z(d_L, H_0)$ is given by the conditional $p(z = z(d_L; H_0) | \beta)$. As the actual redshift prior $p(z | \beta)$ can be a complicated function that models both the unknown evolution of the intrinsic NSBH event rate and also the luminosity-limited selection effect, we will simply assume an uninformative prior. Consequently the hyper-parameter β to parametrize the redshift dependence is also trivial. In this way, the above model likelihood function would be using the NS mass function $\pi(m_{s,2} = m_{o,2} / (1 + z(d_L; H_0)))$ only.

4.3 Assessment of Selection Bias

In a flux-limited survey, the observed luminosity distribution is always biased to the brighter end, so that even if the intrinsic NS mass distribution is symmetric, this selection effect skews the detectable mass distribution. However, as we will show below, this selection effect has only a negligible effect on our results.

Correction for selection bias in GW surveys is difficult, despite the existence of several attempts focused on the binary black hole systems (Messinger & Veitch 2013; Mandel et al. 2019a; Veske et al. 2021). In particular, the full treatment outlined in (Mandel et al. 2019a) also incorporates the Poissonian count noise contributed by finite number of observed events. In our analysis, we ignore the Poissonian noise in order to manage the computational cost. The selection effect for systems involving NS can be more subtle with the extra requirement of quantifying the tidal evolution of the NS during the NSBH merger. In the treatment quantifying selection bias below we also ignore all the extra contribution arisen from tidal effect. In other words, we treat neutron stars as essentially low mass black holes without any internal structure and deformability.

To correct for selection bias, the model term $p(d_L, m_{2,o}, \theta | H_0)$ in Eq. 7 should be modified as the observed data segments $\{D_i\}$ must be passed through the selection criteria, therefore the model term should instead be understood as $p(d_L, m_{o,2}, \theta | H_0, \{D_i \in \text{det}\})$, and we have in fact implicitly included such condition in the likelihood $p(\{D_i\} | d_L, z, \theta, \{D_i \in \text{det}\})$. The importance of bias correction would thus be highlighted by the difference between $p(d_L, m_{o,2}, \theta | H_0, \{D_i \in \text{det}\})$ and $p(d_L, m_{o,2}, \theta | H_0)$.

As \mathcal{M}_c depends also on $m_{s,1}$, the correction for selection bias requires marginalizing over the uncertain black hole mass function $\pi(m_{s,1})$. This can be factorized as:

$$p(d_L, m_{o,2}, \theta | H_0, \{D_i \in \text{det}\}) = \int dm_{s,1} p(d_L, m_{s,1}, m_{o,2}, \theta | H_0, \{D_i \in \text{det}\}) \pi(m_{s,1}) \quad (13)$$

The next step is to expand the term inside the integrand. Conceptually, we would like to cut the parameter subspace which is non-detectable,

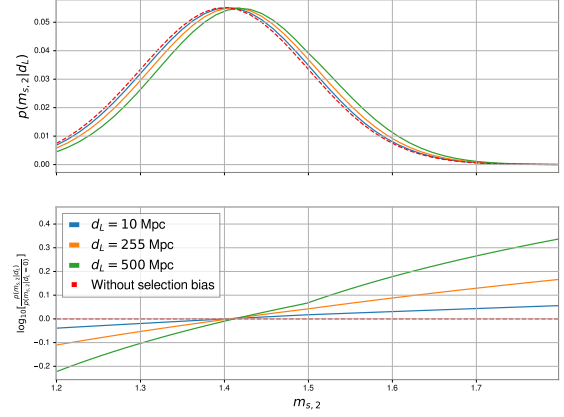


Figure 3. Demonstration of the effect of selection bias. In the upper panel, we show the likelihood of finding mass $m_{s,2}$ at various observed distance d_L . In the lower panel, we show the fractional difference between the mass function with selection bias to the one without the bias (i.e.: the mass function evaluated at $d_L = 0$).

and then we normalize the remaining parameter space to ensure the unity of probability distribution. Symbolically:

$$p(d_L, m_{s,1}, m_{o,2}, \theta | H_0, \{D_i \in \text{det}\}) = \frac{1}{Z} p(d_L, m_{s,1}, m_{o,2}, \theta | H_0) p(\{D_i \in \text{det}\} | d_L, m_{s,1}, m_{o,2}, \theta) \quad (14)$$

Here we model the detection probability $p(\{D_i \in \text{det}\} | d_L, m_{s,1}, m_{o,2}, \theta)$ using the code library GWDET (Gerosa 2017), in which the detection probability calculation are based on spline interpolation among the simulated injection samples defined on grids of points of GW source parameters. We model the biasing effect by $m_{s,1}$ by assuming the BH mass function $\pi(m_{s,1})$ follows the Gaussian + peak model as described in (LIGO-Virgo; LVK, 2021; 2021c), although the detailed choice of $\pi(m_{s,1})$ in (LVK, 2021c) does not significantly change our result we will show. In Figure 3, we compare the expected NS mass function with and without corrected for selection bias. The effect of selection bias can be seen to increase with distance as a higher neutron star mass is necessary to produce sufficient SNR for event detection. The red dotted curve shows the intrinsic NS mass function assumed in this comparison. It is clear that for events in the nearby Universe that the observed NS mass function is not noticeably biased, and this is still the case even we consider events out to the detection limits of approximately $d_L \gtrsim 500$ Mpc, despite a slight potential skew towards the higher masses. Quantitatively, the peak NS mass is shifted only by $0.02 M_\odot$, which corresponds to $\sim 0.2 - 0.4 \sigma_{\text{NS}}$. We conclude that within the current detection horizon of NSBH event of approximately $d_L \approx 800$ Mpc, it is safe to ignore the modest level of selection bias, as the current data quality dominates the current uncertainty budget for H_0 estimated by our method.

In this exploratory work we focus on demonstrating the feasibility of the proposed new measurement method for H_0 and for the rest of the paper, we drop the modelling of selection effect to keep the analysis simple, given the modest level of selection bias we have inferred as the analysis above suggests this selection effect does not have a significant role. Nevertheless we stress that the above scheme for modelling the selection bias can be employed in future analysis

when larger samples of NSBH events are detected for future precision measurements of H_0 at the percent level.

4.4 Results: GW-190426 and GW-200115

With the current limited number of observed NSBH events, inference of H_0 suffers from significant sampling effects, as the NS mass of these events may not fairly represent the underlying NS mass function. The purpose of this current analysis should be understood as a proof of concept, rather than a rigorous inference of H_0 from the existing GW data. In particular, we focus on answering whether with the current signal-to-noise ratio, it is yet possible to deliver any meaningful constraint on H_0 . The main uncertainty currently, as will become clear below, is the distance estimate, d_L derived from the event amplitude, rather than the observed mass $M_c(1+z)$ for which the precision is relatively good for the current NSBH detections. In Figure 5, we show the d_L versus $(1+z)m_2$ posterior for the NSBH events observed so far, with fiducial model assuming different value of H_0 overlaid on the posteriors. As can be seen, the H_0 constraint is substantially worsened by the intrinsic scatter of the NS mass function, and in general, the difference among different H_0 values start to become increasingly distinguishable at long distance d_L . This is also one reason why the use of NSBH is preferred over BNS system. In the plot we also show the posterior of GW190917 in dotted contour, which has an unusual high $m_{s,2}(1+z)$ and is by now the most distant event with extreme mass ratio observed so far.

Using the more secure events as argued in Section 3, namely GW190426_152155 and GW200115_042309, we perform the fitting procedure as outlined above to determine the recent constraint in H_0 . As the scatter in NS mass function is still in debate, we repeat the analysis assuming 4 characteristic value. A fairly broad uniform prior of $H_0 \in [20, 180] \text{ km s}^{-1} \text{ Mpc}^{-1}$ is applied. The result is shown in Figure 4. As the plot indicates, with the very few NSBH events and the poor event-level parameters recovery precision, the constraint on H_0 is not very strong, but a mild exclusion of $H_0 \gtrsim 130 \text{ km s}^{-1} \text{ Mpc}^{-1}$ can be noticed. This is inline with the intuition from Figure 5, where the event posterior contours spread different models assuming different H_0 values. Nonetheless, this demonstrate the applicability of our method. It is promising to notice the method can still deliver some exclusion to H_0 models even with the scarcity of data, which are expected to gradually improve in the near future. A forecast of the improvement in precision, and a study of the systematics will follow in Section 5.

5 FORECASTING NEAR FUTURE PRECISION ON H_0

As the observed number of NSBH events is still limited we now present a forecast to predict the achievable precision on H_0 that can be anticipated in the near future. This is estimated by a dedicated waveform injection pipeline. We perform simulations of NSBH events drawn from an assumed event distribution, and examine how the waveform fitting procedure induces uncertainty in addition to the intrinsic scatter on the NS mass distribution adopted in our prior.

The required modelling for the population of simulated events comprises three distributions, namely: the BH mass function $\pi(m_{s,1})$, the NS mass function $\pi(m_{s,2})$ and the event rate $\pi(z)$. We randomly draw samples from these distribution, and subsequently shifted the source frame quantity $m_{s,1}$, $m_{s,2}$ to the observed frame quantity $m_{o,1}$ and $m_{o,2}$. The $\{m_{o,1}, m_{o,2}, z\}$ samples are then filtered to rule out events that generate weak signal undetectable before

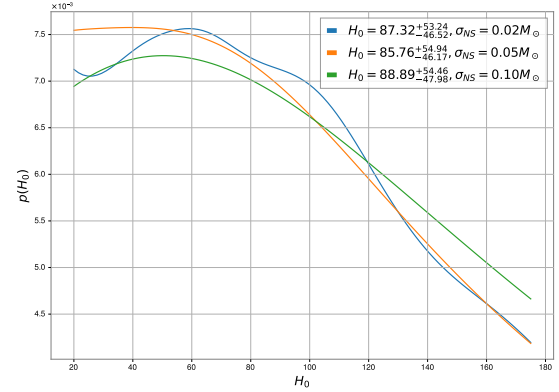


Figure 4. H_0 constraint from the combined constraint of GW-190426 and GW-200115.

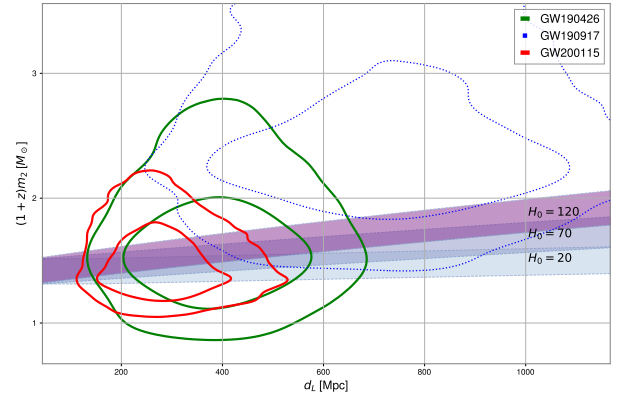


Figure 5. Confidence contour the NSBH events listed in Tab. 1, overplotted with models that assume different values of H_0 (shaded bands). The y-position of the bands is determined by pinning down the the source frame NS mass $m_{s,2} = 1.4 \pm 0.1 M_\odot$, with the boundaries adopting $1.4 + 0.1 M_\odot$ and $1.4 - 0.1 M_\odot$ respectively

any waveform evaluation to cut down the computational cost. Afterwards, we calculate the waveform parametrized only by **observed frame quantities** $\{m_{o,1}, m_{o,2}, d_L\}$ using the publicly available package **BIBLY** (Ashton et al. 2019; Romero-Shaw et al. 2020; Ashton & Talbot 2021), which is the default analysis package for LVK (LVK, 2021) to analysis NSBH event. In particular, we use the approximant *IMRPhenomXPHM* to better handle the extreme mass ratio for NSBH event. We then project the waveform to the detectors LIGO L1, H1 and Virgo, and inject noise realizations to the projected waveform from their corresponding power spectral density. These procedures create simulated observations, namely time series of strain variations among each of the detectors.

These time series are then passed to our fitting pipeline. Our goal is to obtain the H_0 posterior using the simulated time series via Eq. 7. However, as will be explained in the next subsection, we would leave flexibility in choosing the presumed population parameters characterising $\pi(m_{s,2})$. Therefore, the time series would first be fitted assuming a uniform prior in $m_{s,2}$ and z via the MCMC sampler **DYNesty** (Speagle 2020; Ashton & Talbot 2021). We have the freedom to enforce different mass priors $\pi(m_{s,2})$ when the MCMC sam-

ples are subsequently used to calculate H_0 posterior, by re-weighting the MCMC samples as explained in Eq. 10. This approach effectively reduces the undesirable repetitions in MCMC sampling when we switch between priors, and thus cut the computational cost down to a affordable amount. In the fitting procedure, we use the same likelihood function (Pankow et al. 2015) as adopted in LVK analysis (LVK, 2021b). It is numerically implemented in BIBLY, with the phase parameter being analytically marginalized over as demonstrated in (Pankow et al. 2015).

5.1 Event level uncertainty

While the event level parameter recovery and the corresponding uncertainty estimates from noisy signal as been extensively demonstrated by LVK (LVK, 2021b), most of the existing data are on binary BH signals. For our application on NSBH, we would like to focus more on the parameter degeneracy related to z and d_L , and how the correlations varies as switching between different injected event parameters, thus elucidate the limit on H_0 precision due to parameter degeneracy.

5.1.1 Parameter degeneracy

In Section 2, our estimation shows the constraint on z and d_L are inferred from the two (almost independent) observables, namely the chirping spectrum (constrain q and thus $(1+z)m_2$) and the signal amplitude respectively. It is therefore natural to investigate the shape of the posterior given the waveform data: whether the z and d_L are minimally correlated. In Figure 6, we plotted the confidence contours on the d_L and $(1+z)m_2$ plane. If the two parameters are inferred from independent observables, the semi-major and semi-minor axis of the contours should be parallel to the d_L -axis and $(1+z)m_2$ -axis respectively.⁶ Indeed, our intuition is valid. Because of the absence of significant correlation between $(1+z)m_2$ and d_L , we can determine z once m_2 is constrained in the NS mass function defined in the prior. The independent measurement of z and d_L allows one to determine H_0 via the classic Hubble diagram.

5.1.2 BNS vs NSBH

In particular, we would like to understand the advantage of using NSBH over the BNS event to a deeper detail. As argued previously in Section 2 and Eq. 6, due to the efficient amplification powered by the BH companion, NSBH provides the ≈ 4 enlargement of the detection horizon, and thus constrains H_0 much better than BNS.

Recall the precision on constraining H_0 also depends on the estimation uncertainty in z . Apart from the extension of the detection horizon, NSBH also provide tighter estimate on z . Mergers with extreme mass ratio generates waveform that is elongated in time, and thus provide more sample points to improve the estimation on the chirping spectrum which constrains q . To test this intuition, we inject a population of BNS events with both the component masses sampled from the same NS mass function $\pi(m_{s,2})$, and assign the heavier component as m_1 . Similar to what we did for the NSBH events, we fit the injected waveforms using a flat mass prior for both the masses, but adopting the approximant for BNS *IMRPhenomPv2-NRTidal*.

⁶ If the quantites are inferred from correlated observables, the quantites would consequently be linear combinations of all observables. Thus, the covariance matrix would possess off-diagonal terms that tilt the contours at some angle to the d_L -axis and $(1+z)m_2$ axis.

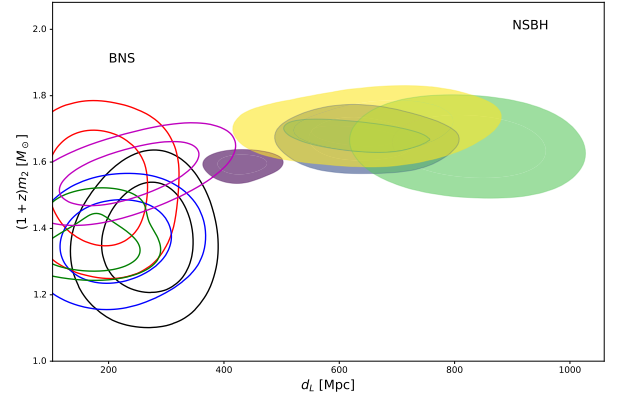


Figure 6. The posterior constraint on 5 simulated BNS (unfilled contours) and NSBH events (filled contours) respectively. Clearly, despite the uncertainty in d_L is slight larger for NSBH, the uncertainty in $(1+z)m_2$ is substantially reduced when compared to BNS event. Therefore a better precision on event redshift z are archived by using NSBH event.

The information of the NS mass function is used only when inferring the H_0 posterior (Eq. 11). Such choice would allow fair comparison among the two types of sources.

The recovered posterior on d_L and $(1+z)m_2$ for each events are plotted in Figure 6. As can be seen, the detectable BNS mostly fall in the more nearby universe, and the associated estimation of $(1+z)m_2$ are more uncertain. In contrary, most NSBH injected are originated at a larger distance as the sampling volume increases. However, the estimation uncertainty in d_L does not worsen significantly. Furthermore, there is a notable improvement in constraining $(1+z)m_2$ and thus z . This demonstrates the advantages for using NSBH over BNS.

5.2 Population level uncertainty

Another limit on precision determination of H_0 comes from (1) the intrinsic scatter of the source population, and (2) the finite sampling from the source distribution.

5.2.1 Sensitivity to source distribution

To examine effect (1), we generate events from $\pi(m_{s,2}; \sigma_{\text{NS}})$ assuming different level of intrinsic scatter σ_{NS} , and feed the simulated data to our fitting pipeline to obtain the posterior $p(H_0 | \{D\})$ following Eq. 10. Note we do not enforce to take the same intrinsic scatter σ_{NS} in the H_0 fitting procedure as in the simulation procedure, hence allowing tests of the sensitivity against incorrect characterization of σ_{NS} .

We injected a population of NSBH with $\langle m_{\text{NS}} \rangle = 1.4M_\odot$ and $\sigma_{\text{NS}}^{(\text{sim})} = 0.1M_\odot$; the large intrinsic scatter of $\sigma_{\text{NS}}^{(\text{sim})} = 0.1M_\odot$ is probably a conservative estimation. We sampled 10 events from the simulation, and determine the H_0 posterior assuming $\sigma_{\text{NS}}^{(\text{fit})} \in \{0.02, 0.05, 0.1, 0.2\}M_\odot$. The Hubble diagram of these simulated events are shown in Figure. 7.

It is clear from Figure 8 that an under-estimated $\sigma_{\text{NS}}^{(\text{fit})} < \sigma_{\text{NS}}^{(\text{sim})}$ would not only lead to the incorrect shrunk of error, but can in principle, substantially shift the mean $\langle H_0 \rangle$ to incorrect value, depending on the sampled mean NS mass $\langle m_{\text{NS}} \rangle^{(\text{fit})}$ in contrast to the simulated mean NS mass $\langle m_{\text{NS}} \rangle^{(\text{sim})}$. An over-estimate of $\sigma_{\text{NS}}^{(\text{fit})} > \sigma_{\text{NS}}^{(\text{sim})}$

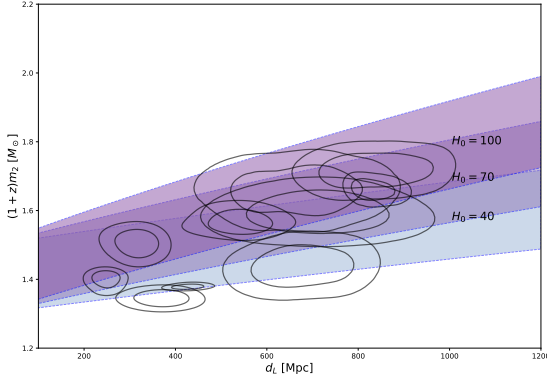


Figure 7. The simulated Hubble Diagrams for the 10 injected events, assuming $\sigma_{\text{NS}} = 0.1 M_{\odot}$.

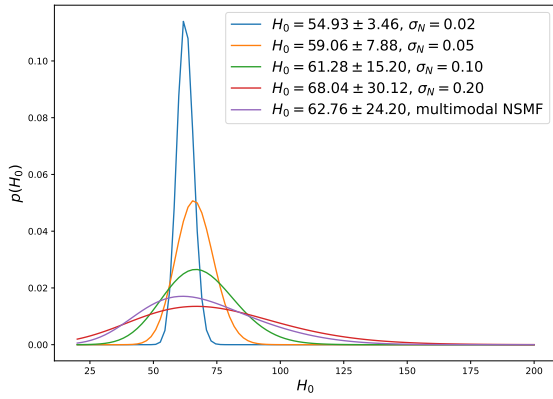


Figure 8. The constraint in H_0 when 10 simulated NSBH events are observed, assuming $\sigma_N^{(\text{sim})} = 0.10 M_{\odot}$. The multimodal neutron star mass function (marked as NSMF on the plot) assumes the two peaks at $m_2 = 1.3$ and $1.5 M_{\odot}$ respectively, with a equal dispersion on each peak $\sigma = 0.1 M_{\odot}$ and equal relative abundance.

tends to diminish such bias effect in the center value of H_0 , but would exaggerate the uncertainty in H_0 .

5.2.2 Source distribution: multimodal

It has been reported that the NS mass distribution is more complicated than a simple Gaussian: instead of a peak around the Chandrasekhar limit $m_{2,s} \sim 1.4 M_{\odot}$, the NS mass function have (at least) two neighboring peaks at $m_{2,s} \approx 1.37 M_{\odot}$ and $1.57 M_{\odot}$ (Zhang et al. 2011) despite the exact location differs in different literatures, depending on the selection of NS samples (see a summary in Section 3, or from (Horvath & Valentim 2017) and reference therein).

As can be seen in Figure 8 (the purple curve therein), the presence of multiple peaks in the NS mass function would in general, skew the distribution towards the direction that corresponds to the less dominant peak. Having said that, the mean value of H_0 can still be recovered. If the peaks in the intrinsic NS mass function are not well separated due to intrinsic scatter, the corresponding H_0 posterior would also hide the peaks due the propagated uncertainty in H_0 .

The reasons for the striking similarity between the multimodal

mass function and the simple Gaussian distribution can be understood as follows. The mean of a two-Gaussians mixture $\Gamma \mathcal{G}(\mu_1, \sigma_1) + (1 - \Gamma) \mathcal{G}(\mu_2, \sigma_2)$, with a relative abundance of $\Gamma \in [0, 1]$, is $\bar{\mu} = \Gamma \mu_1 + (1 - \Gamma) \mu_2$. Similarly, the associated variance is $\bar{\sigma}^2 = \Gamma(\sigma_1^2 + \mu_1^2) + (1 - \Gamma)(\sigma_2^2 + \mu_2^2) - \bar{\mu}^2$. We can statistically assess whether it is possible to significantly distinguish a Gaussian mixture with an effective Gaussian $\mathcal{G}(\bar{\mu}, \bar{\sigma})$ via a two-sample Kolmogorov-Smirnov (KS) test. In particular, we focus on the limit that the number of samples from those distribution are finite, so as to mimic the fact that we would observe limited number of NSBH events. As an visual comparison, we plot a few multimodal mass function with benchmark parameters chosen to mimic some of the claimed form in (Horvath & Valentim 2017). The results are shown in Figure 9. While the appearance of the effective Gaussian description may look very different in terms of the probability distribution function, they look fairly similar in terms of the cumulative distribution function (CDF) - based on which the KS test is built. In particular, the difference is the most noticeable when $\Delta \equiv (\mu_2 - \mu_1)/\min(\sigma_1, \sigma_2) \gg 1$, so that the 2 peaks can be ‘resolved’.

For realistic constraints from the MW observation of NS binaries, $\Delta < 1$, and thus the two description are statistically indistinguishable. This conservative assessment did not take into account of the substantial GW measurement uncertainties in the redshifted NS masses $m_{s,2}$; One would therefore expect the measurement uncertainties would further diminish the difference between the multi-modal distribution and the effective Gaussian. This result is indeed expected: in the effective Gaussian formalism, we force the corresponding mean and variance (the 2 leading statistical moments) to be consistent with the multimodal distribution. Thus, any distinguishable feature would be contributed only starting from the 3-rd order moment, where the amplitude is suppressed at least by $[(x - \bar{\mu})/\bar{\sigma}]^3 \ll 1^3$.

This demonstrates our method is insensitive to the fine detail of the underlying NS mass function, and is therefore robust to the selection of the samples from the electromagnetically observed neutron stars.

5.2.3 Dependence on number of events

Intuitively when the events are completely independent, the uncertainty in H_0 is reduced with increased numbers of events: $\delta^{(N)} H_0 = \frac{1}{\sqrt{N}} \delta^{(1)} H_0$. However, we emphasize that the events are not independent despite the fitting procedures do not rely on the knowledge of other events. The data generation process links the $m_{s,2}$ of each event together via $\pi(m_{s,2})$: the presence of a subset with $m_{s,2} < \langle m_{\text{NS}} \rangle$ implies the likely presence of another subset with $m_{s,2} > \langle m_{\text{NS}} \rangle$, so that the population mean $\langle m_{\text{NS}} \rangle$ is probabilistically restored. The presence of this correlation makes the simple $1/\sqrt{N}$ scaling too optimistic.

To study the impact of those possible hidden correlations, we re-use the simulated events and evaluate the posterior Eq. 10 by supplying randomly sampled subsets of simulated events, with each subset containing different number of events. The results are shown in Figure 10. It is clear that the improvement is slightly slower than $1/\sqrt{N}$, yet the improvement is still significant, so that for example the accumulation of 10 events successfully shrinks the error to 1/2 of the that from a single event, meanwhile driving the posterior mean $\langle H_0 \rangle$ to match the injected value.

5.3 Discussion

As we shown above, shrinking down the H_0 uncertainty innate to this method requires more detected NSBH events, which would be

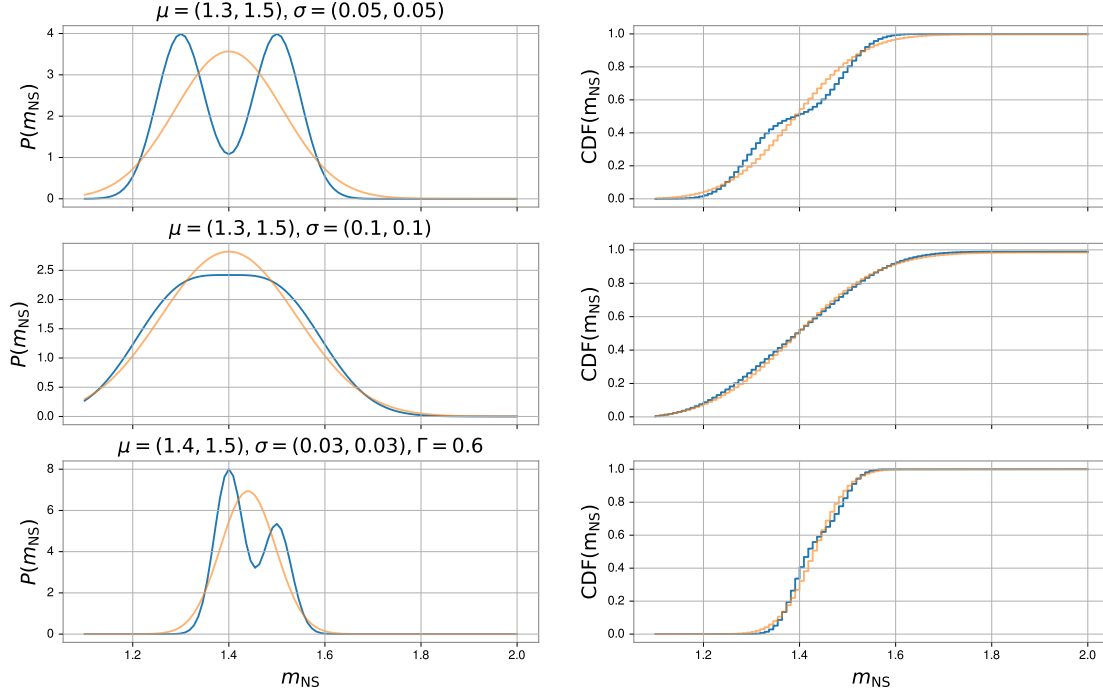


Figure 9. We show the significance of the possible multi-modal feature as reported from some EM observation, and the approximation error for describing the multi-modal distribution by a single effective Gaussian. Three sets of multi-modal parameters are shown in blue line, with the corresponding effective Gaussian plotted in orange. The multi-modal distribution parameters are described in the plot title. On the right column, we show the same comparison, but in terms of the cumulative distribution function (CDF), which are traditionally use to define the distinguishability between distributions (via a Kolmogov-Smirnov test). As can be seen, in terms of the CDF, the effective Gaussian description is highly indifferent from the full, multi-modal description as long as the multi-modal peaks are not largely separated.

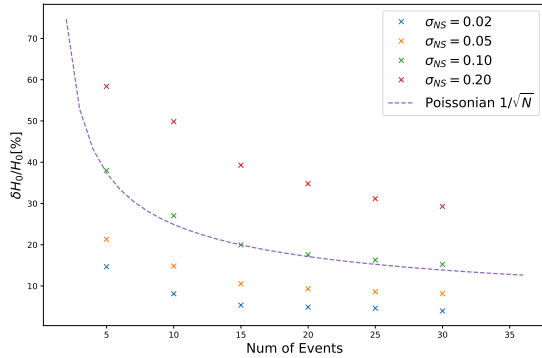


Figure 10. The shrinkage forecast in percentage error in H_0 as a function of number of observed events. It is clear that the shrink in uncertainty improves slightly slower than the Poissonian decay, as the events are not totally independent: they share the calibration parameters (i.e. intrinsic properties of the mass function) in our fitting process.

achievable in the near future. Apart from waiting for more observed NSBH-GW events, other efforts on EM-based observation of the Milky Way NS systems could also help improving the H_0 constraint. One dominant uncertainty is inherited from the estimation of z from the GW data, which require the external, ‘calibration’ input from the

neutron stars observed in the Milky Way. As explained in Section 2 (and the associated schematic Figure 1), once the neutron star mass $m_{s,2}$ is determined, it could be combined with the spectral evolution of the GW events to determine the mass ratio q and thus the source frame chirp mass \mathcal{M}_c . Such source frame chirp mass \mathcal{M}_c can then be compared with the redshifted chirp mass $\mathcal{M}_c(1+z)$ to obtain an estimate of z . On the other hand, there is an independent method to construct a data-driven, external prior on the mass ratio q as well. With an external estimate of q , the uncertainty in the GW spectral evolution constraint on q would significantly shrink.

The EM measurement of mass ratio of binary system involving neutron star is not generally possible, unless at least of the one star of the binary system is a pulsar (or other time-transients). This could be understood as follows: astrometry measurements are able to measure the Keplerian parameters, which constraints the component masses up to an unknown orbit inclination. Such parameter degeneracy can be removed by a companion pulsar - exploiting the relativistic time delay when pulsar signal is deflected by the gravitational field. (See for example, [Lattimer \(2012\)](#) for a review.) Indeed, in the neutron star mass function we picked as demonstration ([Horvath & Valentim 2017](#); [Valentim et al. 2011](#); [Kiziltan et al. 2010](#)), the neutron star mass are obtained from system that hosts at least a pulsar. The measurements of q for each systems allow the construction of the distribution of q . Such externally constraint distribution can then be input as a prior to our analysis pipeline.

Another subtle aspect about the prior on q is to handle its potential

correlation with the mass scale m_{NS} of the corresponding binary system. This is theoretically expected as the formation mechanism of NS with viable mass can be different - possibly including tidal interaction within the binary system where q would be an important control parameter. Owing to limited amount of available of EM-detected NS system, such effect is still unclear; it is also for this reason we stay conservative in this analysis and do not model such effect. However, this should be of practical interest in the near future with the consortium of EM observation and GW observation to lift up such degeneracy, thus help tighten the constraint of H_0 .

A final remark on the application of BNS system, versus the NSBH system as discussed in the current work. As the neutron star mass function has been fixed in *a priori*, in principle the expected chirp mass \mathcal{M}_c can also be fixed by convolving the neutron star mass function with itself. Such process naturally lead to a prior directly on the chirp mass \mathcal{M}_c for BNS system. This is different from the NSBH approach we discussed here - where the primary mass $m_{s,1}$ (black hole mass) and equivalently the mass ratio q has to be constrained by the data. It should be now clear that the BNS approach would strongly influenced by the presumption on the q - m_{NS} correlation, so that the expected chirp mass function is no longer a simple convolution of the neutron star mass function with itself. That is also one reason why NSBH is favoured at the current stage, where the dependence on q is solely addressed by the GW waveform, without exploiting any unclear presumption. Furthermore, the measurement precision for q in NSBH merger is better than is in BNS merger, thanks to the long-lasting waveform during NSBH merger event. However, the synergy of BNS and NSBH to deliver a joint constraint on H_0 is still foreseen in the future upon the rapid accumulation of both EM and GW data.

6 CONCLUSIONS

We have demonstrated here that NSBH events provide an independent and potentially competitive means of estimating H_0 by relying on the characteristic Chandrasekhar mass of neutron stars - using only the GW data, and without the need for a supporting EM redshift. This is thanks to the inherently narrow range of neutron star masses measured to lie in a narrow mass range $m_{\text{NS}} \approx 1.4 \pm 0.1 M_\odot$, provides a simple physically well understood ‘standard siren’ for interpreting the GW waveforms of the GW events of this class. At least one NSBH event is now undisputed, namely GW200115 with a redshifted NS mass of $1.48 M_\odot$ determined in the observer frame from the LVK waveform analysis and with a distances estimated to be $283^{+62.1}_{-82.7}$ Mpc using the measured strain amplitude. Reconsideration of other GW events recorded prior to GW200115 may now be redefined with an NSBH classification, namely event GW190426 and possibly also GW190917 (for which a less conservative ‘prior’ on the rate of NSBH merging is forced by the clear detection of GW200115). Nonetheless we have shown that it is possible to obtain a consistent constraint in H_0 from the existing NSBH events, albeit with larger distance uncertainty due to relatively low SNR in the detections.

We may look forward to upgraded sensitivity that would allow NSBH events with higher SNR, i.e. better defined waveforms for which the degeneracy with orbital/spin parameters can be much improved allowing significantly more precise distance estimation and hence better defined H_0 that will be defined from a joint analysis of a larger sample of future NSBH events. We have emphasised that even with current sensitivity, with only 10 more useful NSBH events we can anticipate $\approx 20\%$.

We have emphasised that this NSBH based method for determining

H_0 is unlike that of BNS events where an external redshift is required for a precision measurement of H_0 , and for which only one BNS case has been detected this way (GW170817) and rather fortuitously via gamma-ray flare time coincidence and the unusually close proximity of this BNS event (GW170817). For NSBH we have the advantage of a much larger detection horizon thanks to the presence of the associated massive black hole that enhances the chirp mass and hence the detectable SNR. Of course for NSBH events with associated EM emission whereby an independent redshift can be established, the precision on H_0 is much improved. Thus it should be regarded as a priority to be prepared for prompt followup of NSBH candidate GW events, but nevertheless this is not a requirement of our method, for which GW alone is sufficient for competitive precision on H_0 at current sensitivities.

REFERENCES

- Ajith P., et al., 2008, *Phys. Rev. D*, 77, 104017
- Ashton G., Talbot C., 2021, *MNRAS*, 507, 2037
- Ashton G., et al., 2019, *ApJS*, 241, 27
- Aubin F., et al., 2021, *Classical and Quantum Gravity*, 38, 095004
- Bassett B. A., Kunz M., 2004, *Phys. Rev. D*, 69, 101305
- Broadhurst T., Diego J. M., Smoot G. F., 2020, Interpreting LIGO/Virgo “Mass-Gap” events as lensed Neutron Star-Black Hole binaries, [doi:10.48550/ARXIV.2006.13219](https://arxiv.org/abs/2006.13219), <https://arxiv.org/abs/2006.13219>
- Camarena D., Marra V., 2021, *MNRAS*, 504, 5164
- Chatterjee D., K. R. A. H., Holder G., Holz D. E., Perkins S., Yagi K., Yunes N., 2021, *Physical Review D*, 104
- Cigarrán Díaz C., Mukherjee S., 2022, *Monthly Notices of the Royal Astronomical Society*, 511, 2782
- Etherington I., 1933, *The London, Edinburgh, and Dublin Philosophical Magazine and Journal of Science*, 15, 761
- Freedman W. L., 2021, *ApJ*, 919, 16
- Freedman W. L., et al., 2019, *The Astrophysical Journal*, 882, 34
- Freedman W. L., et al., 2020, *ApJ*, 891, 57
- Fruchter A. S., Stinebring D. R., Taylor J. H., 1988, *Nature*, 333, 237
- Fung L. W., Li L., Liu T., Luu H. N., Qiu Y.-C., Tye S.-H. H., 2021, *Journal of Cosmology and Astroparticle Physics*, 2021, 057
- Fung L. W. H., Li L., Liu T., Luu H. N., Qiu Y.-C., Tye S. H. H., 2023, *Phys. Rev. Res.*, 5, L022059
- Gerosa D., 2017, *dgerosa/gwdet: v0.1*, [doi:10.5281/zenodo.889966](https://doi.org/10.5281/zenodo.889966), <https://doi.org/10.5281/zenodo.889966>
- Hogg D. W., Myers A. D., Bovy J., 2010, *The Astrophysical Journal*, 725, 2166–2175
- Horvath J. E., Valentim R., 2017, in Alsabti A. W., Murdin P., eds., *Handbook of Supernovae*. p. 1317, [doi:10.1007/978-3-319-21846-5_67](https://doi.org/10.1007/978-3-319-21846-5_67)
- Ivanov M. M., Ali-Haïmoud Y., Lesgourgues J., 2020, *Physical Review D*, 102
- Jedamzik K., Pogosian L., Zhao G.-B., 2021, *Communications Physics*, 4
- Kandel D., Romani R. W., 2022, *The Astrophysical Journal*, 942, 6
- Kiziltan B., Kottas A., Thorsett S. E., 2010, The Neutron Star Mass Distribution, [doi:10.48550/ARXIV.1011.4291](https://arxiv.org/abs/1011.4291), <https://arxiv.org/abs/1011.4291>
- Kiziltan B., Kottas A., Yoreo M. D., Thorsett S. E., 2013, *The Astrophysical Journal*, 778, 66
- Knox L., Millea M., 2020, *Physical Review D*, 101
- LIGO Scientific Collaboration Virgo Collaboration 2021, *ApJ*, 913, L7
- LIGO Scientific Collaboration and Virgo Collaboration 2017a, *Phys. Rev. Lett.*, 119, 161101
- LIGO Scientific Collaboration and Virgo Collaboration 2017b, *Nature*, 551, 85
- LIGO-Virgo-Kagra collaboration 2021, *The Astrophysical Journal Letters*, 915, L5
- LIGO collaboration 2020, *Phys. Rev. D*, 102, 062003

- Lattimer J. M., 2012, *Annual Review of Nuclear and Particle Science*, 62, 485
- Li Y.-J., Han M.-Z., Tang S.-P., Wang Y.-Z., Hu Y.-M., Yuan Q., Fan Y.-Z., Wei D.-M., 2020, GW190426-152155: a merger of neutron star-black hole or low mass binary black holes?, doi:10.48550/ARXIV.2012.04978, <https://arxiv.org/abs/2012.04978>
- Luu H. N., 2021, Axi-Higgs cosmology: Cosmic Microwave Background and cosmological tensions, doi:10.48550/ARXIV.2111.01347, <https://arxiv.org/abs/2111.01347>
- Mandel I., Farr W. M., Gair J. R., 2019a, *Monthly Notices of the Royal Astronomical Society*, 486, 1086
- Mandel I., Farr W. M., Gair J. R., 2019b, *Monthly Notices of the Royal Astronomical Society*, 486, 1086–1093
- Messenger C., Veitch J., 2013, *New Journal of Physics*, 15, 053027
- Mukherjee S., Wandelt B. D., Nissanke S. M., Silvestri A., 2021, *Physical Review D*, 103
- Nissanke S., Holz D. E., Dalal N., Hughes S. A., Sievers J. L., Hirata C. M., 2013, Determining the Hubble constant from gravitational wave observations of merging compact binaries, doi:10.48550/ARXIV.1307.2638, <https://arxiv.org/abs/1307.2638>
- Oguri M., 2016, *Physical Review D*, 93
- Pankow C., Brady P., Ochsner E., O’Shaughnessy R., 2015, *Physical Review D*, 92
- Planck Collaboration et al., 2020, *A&A*, 641, A6
- Poisson E., Will C. M., 1995, *Physical Review D*, 52, 848
- Riess A. G., et al., 2021, A Comprehensive Measurement of the Local Value of the Hubble Constant with 1 km/s/Mpc Uncertainty from the Hubble Space Telescope and the SH0ES Team, doi:10.48550/ARXIV.2112.04510, <https://arxiv.org/abs/2112.04510>
- Romani R. W., Filippenko A. V., Silverman J. M., Cenko S. B., Greiner J., Rau A., Elliott J., Pletsch H. J., 2012, *ApJ*, 760, L36
- Romero-Shaw I. M., et al., 2020, *MNRAS*, 499, 3295
- Schutz B. F., 1986, *Nature*, 323, 310
- Scolnic D. M., et al., 2018, *The Astrophysical Journal*, 859, 101
- Speagle J. S., 2020, *MNRAS*, 493, 3132
- The LIGO Scientific Collaboration The Virgo Collaboration 2021, GWTC-2.1: Deep Extended Catalog of Compact Binary Coalescences Observed by LIGO and Virgo During the First Half of the Third Observing Run, doi:10.48550/ARXIV.2108.01045, <https://arxiv.org/abs/2108.01045>
- The LIGO Scientific Collaboration The Virgo Collaboration The KAGRA Collaboration 2021a, Constraints on the cosmic expansion history from GWTC-3, doi:10.48550/ARXIV.2111.03604, <https://arxiv.org/abs/2111.03604>
- The LIGO Scientific Collaboration The Virgo Collaboration The KAGRA Collaboration 2021b, GWTC-3: Compact Binary Coalescences Observed by LIGO and Virgo During the Second Part of the Third Observing Run, doi:10.48550/ARXIV.2111.03606, <https://arxiv.org/abs/2111.03606>
- The LIGO Scientific Collaboration the Virgo Collaboration the KAGRA Collaboration 2021c, arXiv e-prints, p. arXiv:2111.03634
- Thorsett S. E., Chakrabarty D., 1999, *ApJ*, 512, 288
- Valentin R., Rangel E., Horvath J. E., 2011, *Monthly Notices of the Royal Astronomical Society*, 414, 1427
- Valentino E. D., et al., 2021, *Classical and Quantum Gravity*, 38, 153001
- Verde L., Treu T., Riess A. G., 2019, *Nature Astronomy*, 3, 891
- Veske D., Bartos I., Márka Z., Márka S., 2021, *The Astrophysical Journal*, 922, 258
- Zhang C. M., et al., 2011, *Astronomy & Astrophysics*, 527, A83

the likelihood. The method relies on the factorization of extrinsic parameters (in particular, d_L) and intrinsic parameters (m_c, η). As the effect of extrinsic parameters are shiftings and scalings of the waveform, in contrary to the expensive differential equation solvers involved for intrinsic parameters, analytical marginalization over extrinsic parameters are allowed.

For almost the same reason, the aforementioned data pipeline does not take the redshift as input, templates evaluated at any distance are not redshift corrected, thus the corresponding output intrinsic parameters \mathcal{M}_c are instead the redshift-uncorrected parameters. The MCMC samples provided by LVK determine only the distance d_L , the redshift samples are not used in the waveform fitting at all, and is obtained via trivially applying the assumed P18 cosmology with $H_0 = 67.9 \text{ km s}^{-1} \text{ Mpc}^{-1}$.

This paper has been typeset from a \LaTeX file prepared by the author.

APPENDIX A: REMARKS ON LVK LIKELIHOOD EVALUATION

We note that the `pycbc` and `BILBY` GW parameters inference package used the accelerated method outlined in (Pankow et al. 2015) to compare between model templates and the data, and thus evaluating